Single-particle properties and pseudogap effects in the BCS-BEC crossover regime of an ultracold Fermi gas above T_c

Shunji Tsuchiya,[1,2] Ryota Watanabe,[1] and Yoji Ohashi[1,2]
[1]*Department of Physics, Keio University, 3-14-1 Hiyoshi, Kohoku-ku, Yokohama 223-8522, Japan*
[2]*CREST, JST, 4-1-8 Honcho, Saitama 332-0012, Japan*
(Received 27 July 2009; published 16 September 2009)

We investigate strong-coupling effects on normal-state properties of an ultracold Fermi gas. Within the framework of T-matrix approximation in terms of pairing fluctuations, we calculate the single-particle density of states (DOS), as well as the spectral weight, over the entire BCS–Bose-Einstein condensate (BEC) crossover region above the superfluid phase-transition temperature T_c. Starting from the weak-coupling BCS regime, we show that the so-called pseudogap develops in DOS above T_c, which becomes remarkable in the crossover region. The pseudogap structure continuously changes into a fully gapped one in the strong-coupling BEC regime, where the gap energy is directly related to the binding energy of tightly bound molecules. We determine the pseudogap temperature T^* where the dip structure in DOS vanishes. The value of T^* is shown to be very different from another characteristic temperature T^{**} where a BCS-type double-peak structure disappears in the spectral weight. While one finds $T^*>T^{**}$ in the BCS regime, T^{**} becomes higher than T^* in the crossover region and BEC regime. Including this, we determine the pseudogap region in the phase diagram of ultracold Fermi gases. Our results would be useful in the search for the pseudogap region in ultracold ^{6}Li and ^{40}K Fermi gases.

DOI: 10.1103/PhysRevA.80.033613 PACS number(s): 03.75.Ss, 05.30.Fk, 67.85.−d

I. INTRODUCTION

Ultracold atomic Fermi gases provide unique opportunities to investigate the crossover from the Bardeen-Cooper-Schrieffer (BCS)-type superfluids to the Bose-Einstein condensates (BECs) of tightly bound molecules [1–4] in a unified manner [5–9]. One of the key ingredients to achieve this BCS-BEC crossover in Fermi gases is a Feshbach resonance [9], which allows one to tune the pairing interaction from the weak-coupling BCS limit to the strong-coupling BEC limit [10–14]. Since the BCS-BEC crossover is a fundamental many-body problem, it has recently attracted much attention, not only in cold atom physics, but also in various research fields, such as condensed-matter physics and high-energy physics. In particular, this system is expected to be helpful for further understanding of high-T_c cuprates, which has been one of the most challenging problems in condensed-matter physics [15].

In the underdoped regime of high-T_c cuprates, the so-called pseudogap phenomenon has been extensively studied [15,16]. In this phenomenon, the single-particle density of states (DOS) in the normal state exhibits a dip structure around the Fermi energy. The temperature at which the pseudogap appears is referred to as the pseudogap temperature T^*, which is higher than the superconducting phase-transition temperature T_c. In the region between T^* and T_c, various anomalies have been observed in physical quantities, such as nuclear spin-lattice relaxation rate (NMR T_1^{-1}) [17] and angle-resolved photoemission spectroscopy [18]. As the origin of the pseudogap, the possibility of preformed pairs due to strong pairing fluctuations has been proposed [19–24]. However, because of the complexity of high-T_c cuprates, other scenarios have been also discussed, such as antiferromagnetic spin fluctuations [25,26] and a hidden order [27]. Thus, a simple system only having strong pairing fluctuations would be helpful to confirm whether or not preformed pairs are responsible for the pseudogap formation in high-T_c cuprates.

In this regard, the cold Fermi gas system meets this demand. This system is much cleaner and simpler than high-T_c cuprates, and the pairing mechanism associated with a Feshbach resonance has been well understood. The BCS-BEC crossover is dominated by strong pairing fluctuations, so that one can focus on how they affect physical quantities. Indeed, effects of pairing fluctuations on single-particle spectral weight have been theoretically studied by many researchers [21–24,28–32]. They clarified that pairing fluctuations lead to a BCS-type double-peak structure in the spectral weight above T_c, which is a signature of pseudogap phenomenon. They also found that the two peaks in the spectral weight merge into a single peak at high temperatures. In Ref. [24], detailed analysis on the spectral weight above T_c has been carried out over the entire BCS-BEC crossover and, in the BEC regime, the deviation from the BCS-type behaviors due to an asymmetric double-peak structure has been pointed out. Since a photoemission-type experiment has recently become possible in cold atom physics [33], we can now examine strong-coupling effects on single-particle excitations within the current experimental technology. Although cold Fermi gases are not exactly the same as high-T_c cuprates (e.g., pairing symmetry), the study of pseudogap phenomenon in cold Fermi gases is expected to be useful for further understanding of the underdoped regime of high-T_c cuprates.

In this paper, we investigate pseudogap behaviors of an ultracold Fermi gas above T_c. Including pairing fluctuations within the T-matrix approximation developed in Refs. [22,24], we systematically examine how the pseudogap develops in DOS, as well as the spectral weight, over the entire BCS-BEC crossover region. We determine the pseudogap temperature T^* at which the dip structure in DOS vanishes.

We show that T^* is quite different from the temperature T^{**} where the double-peak structure in the spectral weight disappears. In the BCS regime, we find that $T^* > T^{**}$. However, T^{**} becomes higher than T^* in the crossover region and BEC regime. Including this, we determine the pseudogap region in the BCS-BEC crossover phase diagram in terms of the temperature and the strength of pairing interaction.

This paper is organized as follows. In Sec. II, we explain our model and formulation to study pseudogap in DOS and spectral weight. In Sec. III, we examine the pseudogap structure in DOS. Here, we show how the pseudogapped DOS continuously changes into fully gapped one, as one passes through the BCS-BEC crossover region. We determine the pseudogap temperature T^* from the temperature dependence of DOS. In Sec. IV, we examine strong-coupling effects on the spectral weight. We introduce another pseudogap temperature T^{**} from the temperature dependence of spectral weight. We also discuss the difference between T^* and T^{**}. Throughout this paper, we take $\hbar = k_B = 1$.

II. MODEL AND FORMALISM

We consider a three-dimensional uniform Fermi gas, consisting of two atomic hyperfine states described by pseudospin $\sigma = \uparrow, \downarrow$. So far, all the experiments on cold Fermi gases are using a broad Feshbach resonance to tune the strength of a pairing interaction [5–9]. In this case, a detailed Feshbach-induced pairing mechanism is known to be not crucial as far as we consider the interesting BCS-BEC crossover regime, and one can safely use the ordinary single-channel BCS model, described by the Hamiltonian

$$H = \sum_{\boldsymbol{p},\sigma} \xi_{\boldsymbol{p}} c^\dagger_{\boldsymbol{p}\sigma} c_{\boldsymbol{p}\sigma} - U \sum_{\boldsymbol{q}} \sum_{\boldsymbol{p},\boldsymbol{p}'} c^\dagger_{\boldsymbol{p}+\boldsymbol{q}/2\uparrow} c^\dagger_{-\boldsymbol{p}+\boldsymbol{q}/2\downarrow} c_{-\boldsymbol{p}'+\boldsymbol{q}/2\downarrow} c_{\boldsymbol{p}'+\boldsymbol{q}/2\uparrow}. \tag{1}$$

Here, $c_{\boldsymbol{p}\sigma}$ is the annihilation operator of a Fermi atom with the pseudospin σ and the kinetic energy $\xi_{\boldsymbol{p}} = \varepsilon_{\boldsymbol{p}} - \mu = p^2/2m - \mu$, measured from the chemical potential μ (where m is an atomic mass). $-U$ (<0) is an assumed tunable pairing interaction associated with a Feshbach resonance. It is related to the s-wave scattering length a_s as [34]

$$\frac{4\pi a_s}{m} = -\frac{U}{1 - U\sum_{\boldsymbol{p}}^{\omega_c} \frac{1}{2\varepsilon_{\boldsymbol{p}}}}, \tag{2}$$

where ω_c is a high-energy cutoff. Since the strength of an interaction is usually measured in terms of the scattering length a_s in cold atom physics, Eq. (2) is useful in comparing theoretical results with experiments. In this scale, the weak-coupling BCS limit and strong-coupling BEC limit are characterized as $(k_F a_s)^{-1} \ll -1$ and $(k_F a_s)^{-1} \gg +1$, respectively (where k_F is the Fermi momentum). The region $-1 \lesssim (k_F a_s)^{-1} \lesssim +1$ is referred to as the crossover region. The center of the crossover region $[(k_F a_s)^{-1} = 0]$ is called the unitarity limit [35].

To discuss strong-coupling effects in the BCS-BEC crossover regime above T_c, we include pairing fluctuations within the T-matrix approximation [22,24]. Namely, we consider the single-particle thermal Green's function [36]

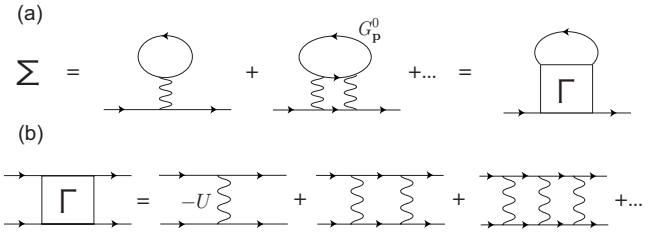

FIG. 1. (a) Self-energy correction $\Sigma(\boldsymbol{p}, i\omega_n)$ and (b) particle-particle scattering matrix $\Gamma(\boldsymbol{q}, i\nu_n)$ in the T-matrix approximation. The solid and wavy lines represent the noninteracting Fermi Green's function $G^0_{\boldsymbol{p}}(i\omega_n)$ and pairing interaction $-U$, respectively.

$$G_{\boldsymbol{p}}(i\omega_n) = \frac{1}{i\omega_n - \xi_{\boldsymbol{p}} - \Sigma(\boldsymbol{p}, i\omega_n)}, \tag{3}$$

where ω_n is the fermion Matsubara frequency. The self-energy correction $\Sigma(\boldsymbol{p}, i\omega_n)$ describes effects of pairing fluctuations, which is diagrammatically given by Fig. 1(a). In Fig. 1, the solid lines are the free fermion propagator

$$G^0_{\boldsymbol{p}}(i\omega_n) = \frac{1}{i\omega_n - \xi_{\boldsymbol{p}}}. \tag{4}$$

Although this T-matrix theory does not treat the single-particle Green's function self-consistently, Ref. [24] has shown that it can correctly describe the smooth crossover from the BCS regime to the BEC regime. We briefly note that the self-consistent T-matrix approximation (where the full Green's function G is used instead of G^0 in evaluating the self-energy) has been recently employed to study the spectral weight and the rf spectrum in the crossover region [32].

Summing up the diagrams in Fig. 1(a), we obtain

$$\Sigma(\boldsymbol{p}, i\omega_n) = T\sum_{\boldsymbol{q},\nu_n} \Gamma(\boldsymbol{q}, i\nu_n) G^0_{\boldsymbol{q}-\boldsymbol{p}}(i\nu_n - i\omega_n) e^{i(\nu_n - \omega_n)\delta}, \tag{5}$$

where ν_n is the boson Matsubara frequency. The particle-particle scattering matrix $\Gamma(\boldsymbol{q}, i\nu_n)$, which describes fluctuations in the Cooper channel, is diagrammatically given by Fig. 1(b). The expression is given by

$$\Gamma(\boldsymbol{q}, i\nu_n) = \frac{-U}{1 - U\Pi(\boldsymbol{q}, i\nu_n)} = \frac{4\pi a_s}{m} \frac{1}{1 + \frac{4\pi a_s}{m}\left[\Pi(\boldsymbol{q}, i\nu_n) - \sum_{\boldsymbol{p}} \frac{1}{2\varepsilon_{\boldsymbol{p}}}\right]}. \tag{6}$$

In the last expression, the ultraviolet divergence coming from the contact pairing interaction has been absorbed into the scattering length a_s [34]. $\Pi(\boldsymbol{q}, i\nu_n)$ is the pair propagator given by

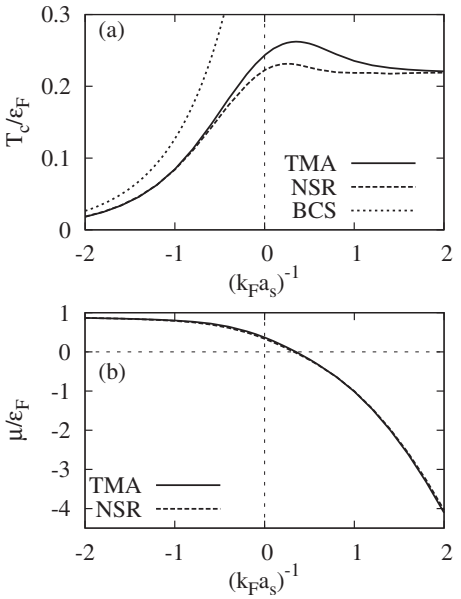

FIG. 2. Self-consistent solutions of the coupled Eqs. (8) and (9) in the BCS-BEC crossover ("TMA" in the figure). (a) Phase-transition temperature T_c. (b) Chemical potential $\mu(T=T_c)$. In (b), μ is negative when $(k_Fa_s)^{-1} \geq 0.35$. "BCS" and "NSR" are the weak-coupling BCS and the NSR results, respectively.

$$\Pi(\boldsymbol{q}, i\nu_n) = T\sum_{\boldsymbol{p},\omega_n} G^0_{\boldsymbol{p}+\boldsymbol{q}/2}(i\nu_n + i\omega_n)G^0_{-\boldsymbol{p}+\boldsymbol{q}/2}(-i\omega_n)$$
$$= \sum_{\boldsymbol{p}} \frac{1 - f(\xi_{\boldsymbol{p}+\boldsymbol{q}/2}) - f(\xi_{\boldsymbol{p}-\boldsymbol{q}/2})}{\xi_{\boldsymbol{p}+\boldsymbol{q}/2} + \xi_{\boldsymbol{p}-\boldsymbol{q}/2} - i\nu_n}, \tag{7}$$

where $f(\varepsilon)$ is the Fermi distribution function.

To examine the pseudogap region, one needs to determine T_c [3,4,12,24]. The equation for T_c is obtained from the Thouless criterion [8] $\Gamma(\boldsymbol{q}=0,\ i\nu_n=0,\ T=T_c)^{-1}=0$, which gives

$$1 = -\frac{4\pi a_s}{m}\sum_{\boldsymbol{p}}\left[\frac{1}{2(\varepsilon_{\boldsymbol{p}} - \mu)}\tanh\frac{\xi_{\boldsymbol{p}}}{2T} - \frac{1}{2\varepsilon_{\boldsymbol{p}}}\right]. \tag{8}$$

As pointed out by Nozières and Schmitt-Rink (NSR) [3], the chemical potential μ deviates from the Fermi energy ε_F in the BCS-BEC crossover. This strong-coupling effect can be conveniently included by solving Eq. (8), together with the equation for the number N of Fermi atoms

$$N = 2T\sum_{\boldsymbol{p},\omega_n} e^{i\omega_n\delta}G_{\boldsymbol{p}}(i\omega_n). \tag{9}$$

We show the self-consistent solutions of the coupled equations (8) and (9) in Fig. 2.

In the normal phase above T_c, we only solve the number equation (9) to determine the temperature dependence of $\mu(T>T_c)$. The resulting $\mu(T)$ in Fig. 3 is used to calculate DOS $\rho(\omega)$, as well as the spectral weight $A(\boldsymbol{p},\omega)$. They are obtained from the analytical continued Green's function as, respectively,

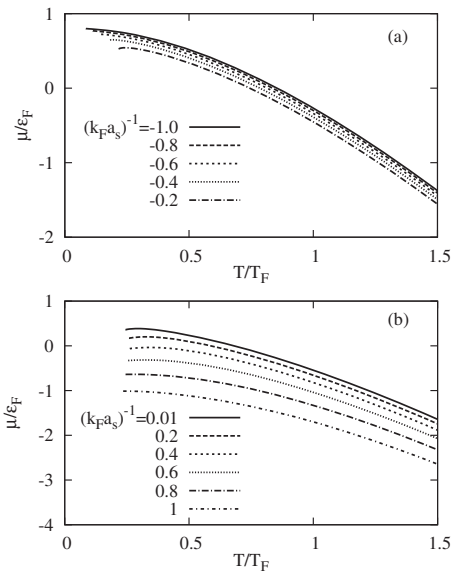

FIG. 3. Calculated chemical potential μ above T_c in the (a) BCS and (b) BEC sides. Each line starts from T_c. We will use these results in calculating the density of states and spectral weight in Secs. III and IV.

$$\rho(\omega) = -\frac{1}{\pi}\sum_{\boldsymbol{p}} \mathrm{Im}[G(\boldsymbol{p}, i\omega \to \omega + i\delta)], \tag{10}$$

$$A(\boldsymbol{p},\omega) = -\frac{1}{\pi}\mathrm{Im}[G(\boldsymbol{p}, i\omega \to \omega + i\delta)]. \tag{11}$$

The analytical continued self-energy in $G(\boldsymbol{p}, i\omega_n \to \omega + i\delta)$ has the form

$$\Sigma(\boldsymbol{p}, \omega + i\delta) = \Sigma_{\mathrm{H}} + \frac{1}{\pi}\sum_{\boldsymbol{q}}\int_{-\infty}^{\infty} dz \frac{n_B(z) + f(\xi_{\boldsymbol{q}-\boldsymbol{p}})}{z - (\omega + i\delta) - \xi_{\boldsymbol{q}-\boldsymbol{p}}}$$
$$\times \mathrm{Im}[\Gamma(\boldsymbol{q}, i\nu_n \to z + i\delta)], \tag{12}$$

where $n_B(\varepsilon)$ is the Bose distribution function. $\Sigma_{\mathrm{H}} = -(U/2)\Sigma_{\boldsymbol{p}} f(\xi_{\boldsymbol{p}})$ is the Hartree term and the last term in Eq. (12) describes the fluctuation correction to single-particle excitations.

Before ending this section, we comment on the T-matrix theory used in this paper. In the BCS-BEC crossover literature, the so-called Gaussian fluctuation theory developed by NSR [3,4] has been also used. The present T-matrix theory is a natural extension of this to include higher-order pairing fluctuations. Indeed, the T_c [Eq. (8)] is common to the two theories and the NSR number equation is also obtained from Eq. (9), by expanding $G_{\boldsymbol{p}}(i\omega_n)$ in Eq. (9) up to $O(\Sigma)$, as

$$G^{\mathrm{NSR}}_{\boldsymbol{p}}(i\omega_n) = G^0_{\boldsymbol{p}}(i\omega_n) + G^0_{\boldsymbol{p}}(i\omega_n)\Sigma(\boldsymbol{p}, i\omega_n)G^0_{\boldsymbol{p}}(i\omega_n). \tag{13}$$

The two theories essentially give the same BCS-BEC crossover behaviors of T_c and $\mu(T=T_c)$, as shown in Fig. 2. In particular, both theories correctly describe the strong-coupling BEC limit, where the superfluid phase transition is dominated by BEC of $N/2$ tightly bound molecules (which leads to $T_c = 0.218T_F$ [3]) and $2|\mu|$ equals the binding energy of a two-body bound state $E_{\mathrm{bind}} = 1/ma_s^2$ [2]. However, when

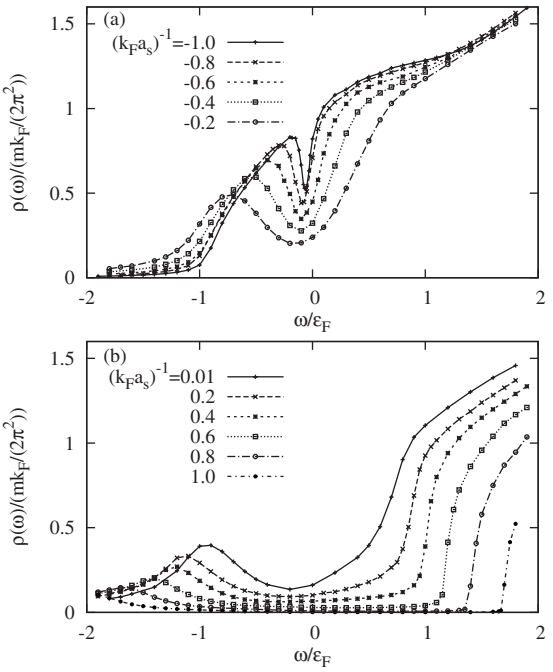

FIG. 4. Density of states at T_c. (a) BCS side $[(k_F a_s)^{-1} < 0]$. (b) BEC side $[(k_F a_s)^{-1} > 0]$.

one uses $G_p^{\mathrm{NSR}}(i\omega_n \to \omega + i\delta)$ in calculating Eq. (10), unphysical results are obtained. The NSR theory overestimates the suppression of DOS around $\omega=0$, leading to a negative DOS around $\omega=0$ in the crossover region [37]. The NSR theory also gives an unphysical divergence of DOS at $\omega=\mu$ (although we do not explicitly show this in this paper) [37]. Thus, although the NSR theory can describe the BCS-BEC crossover behaviors of T_c and μ, one needs to be careful in considering single-particle properties in the BCS-BEC crossover. Since this problem is absent in the present T-matrix theory, we employ this framework to examine the DOS and the spectral weight in this paper.

III. PSEUDOGAP IN SINGLE-PARTICLE DENSITY OF STATES

In this section, we discuss the pseudogap phenomenon in DOS. Figure 4 shows DOS in the BCS-BEC crossover at T_c. Starting from the weak-coupling BCS regime, a pseudogap develops around $\omega=0$ as one increases the strength of the pairing interaction. Since the superfluid order parameter vanishes at T_c, this dip structure purely originates from pairing fluctuations.

The reason why the fluctuation correction described by the self-energy in Eq. (3) causes the pseudogap in DOS can be easily understood by noting the similarity between Eq. (3) and the Green's function in the mean-field BCS theory [38]

$$G_p^{\mathrm{BCS}}(i\omega_n) = -\frac{i\omega_n + \xi_p}{\omega_n^2 + \xi_p^2 + \Delta^2}, \tag{14}$$

where Δ is the superfluid order parameter. Assuming that pairing fluctuations are strong around $\boldsymbol{q}=\nu_n=0$ [note that $\Gamma(\boldsymbol{q}=0,\ \nu_n=0)$ diverges at T_c], we may approximate Eq. (5) to

$$\Sigma(\boldsymbol{p}, i\omega_n) \simeq \Sigma_{\mathrm{H}} - G_{-\boldsymbol{p}}^0(-i\omega_n)\Delta_{\mathrm{pg}}^2, \tag{15}$$

where $\Delta_{\mathrm{pg}}^2 \equiv -T\Sigma_{\boldsymbol{q},\nu_n}[\Gamma(\boldsymbol{q}, i\nu_n) + U]$. Although $G_{-\boldsymbol{p}}^0$ in Eq. (15) does not involve the Hartree term Σ_{H} in the present T-matrix approximation, a better approximation would involve it in evaluating Σ. In this case, substituting Eq. (15) into Eq. (3), we obtain

$$G_{\boldsymbol{p}}(i\omega_n) = \frac{1}{i\omega_n - \xi_{\boldsymbol{p}} + \Delta_{\mathrm{pg}}^2 G_{-\boldsymbol{p}}^0(-i\omega_n)} = -\frac{i\omega_n + \xi_{\boldsymbol{p}}}{\omega_n^2 + \xi_{\boldsymbol{p}}^2 + \Delta_{\mathrm{pg}}^2}, \tag{16}$$

where μ in $\xi_{\boldsymbol{p}}$ is replaced with $\mu + \Sigma_{\mathrm{H}}$. Since $G_{-\boldsymbol{p}}^0(-i\omega_p)$ may be regarded as the hole Green's function, Eq. (16) means that pairing fluctuations induce a particle-hole coupling. Comparing Eq. (16) with Eq. (14), we find that Δ_{pg} (which describes effects of pairing fluctuations) plays the same role as the BCS gap parameter Δ. Actually, dynamical effects of pairing fluctuations with $\boldsymbol{q} \neq 0$ and $\nu_n \neq 0$ smear the clear gap structure and coherence peak known in the mean-field BCS theory. However, in Fig. 4(a), one can still see broad peaks around $\omega/\varepsilon_F \simeq \pm 0.2$ (which corresponds to the diverging coherence peaks at $\omega = \pm\Delta$ in the BCS theory) when $(k_F a_s)^{-1} \lesssim -0.4$. Although the above discussion simplifies the treatment of pairing fluctuations, it would be helpful in understanding the reason why pairing fluctuations give the pseudogap structure above T_c.

While the pseudogapped DOS is very remarkable in the unitarity limit, it continuously changes into a *fully* gapped one in the strong-coupling BEC regime, as shown in Fig. 4(b). In the BEC regime where μ is negative $[(k_F a_s)^{-1} > 0.35]$, when we only retain the negative μ and ignore other strong-coupling effects, the DOS has a finite energy gap $|\mu|$ as

$$\rho(\omega) = \begin{cases} 0 & (\omega < |\mu|) \\ \dfrac{m^{3/2}}{\sqrt{2}\pi^2}\sqrt{\omega - |\mu|} & (\omega \geq |\mu|). \end{cases} \tag{17}$$

In the BEC limit, $2|\mu|$ equals the binding energy $E_{\mathrm{bind}} = 1/ma_s^2$ of a two-body bound state, which means that the energy gap in Eq. (17) is directly related to the molecular dissociation energy. Since the intensity of DOS is almost absent below $\omega/\varepsilon_F \sim 1.4$ when $(k_F a_s)^{-1} = +0.8$ in Fig. 4(b), the region of $(k_F a_s)^{-1} \gtrsim 0.8$ is considered to be close to an $N/2$ molecular gas, rather than an N atomic Fermi gas.

However, we note that $\rho(\omega<0)$ still has small but *finite* intensity even when $(k_F a_s)^{-1} \gtrsim 1.0$, as shown in Fig. 4(b), which means the existence of hole-type excitations. The finite DOS in the negative-energy region is absent when we ignore all fluctuation effects except for the negative μ [see Eq. (17)]. Since the concept of hole is characteristic of many-fermion system, one finds that, although the BEC region around $(k_F a_s)^{-1} \simeq +1$ is dominated by two-body molecular *bosons*, the character of many-fermion system still remains to some extent there, leading to the finite $\rho(\omega<0)$. We also find this by simply employing Eq. (16) to calculate DOS in the BEC regime $(\mu<0)$, which gives

$$\rho(\omega)=\begin{cases}\dfrac{m^{3/2}}{2\sqrt{2}\pi^2}\dfrac{\omega}{\sqrt{\omega^2-\Delta_{\rm pg}^2}}\left[1+\dfrac{\sqrt{\omega^2-\Delta_{\rm pg}^2}}{\omega}\right]\sqrt{\sqrt{\omega^2-\Delta_{\rm pg}^2}-|\mu|} & (\omega\geq\sqrt{\Delta_{\rm pg}^2+|\mu|^2}) \\ \dfrac{m^{3/2}}{2\sqrt{2}\pi^2}\dfrac{|\omega|}{\sqrt{\omega^2-\Delta_{\rm pg}^2}}\left[1-\dfrac{\sqrt{\omega^2-\Delta_{\rm pg}^2}}{|\omega|}\right]\sqrt{\sqrt{\omega^2-\Delta_{\rm pg}^2}-|\mu|} & (\omega\leq-\sqrt{\Delta_{\rm pg}^2+|\mu|^2}).\end{cases} \tag{18}$$

When the two-body binding energy $E_{\rm bind}=1/ma_s^2(\simeq 2|\mu|)$ is much larger than the "characteristic energy" $\Delta_{\rm pg}$, one may ignore $\Delta_{\rm pg}$ in Eq. (18). In this extreme BEC limit, the upper branch in Eq. (18) reduces to Eq. (17), and the lower one vanishes, as expected.

Figures 5 and 6 show DOS above T_c. The pseudogap structure in DOS becomes obscure at high temperatures due to weak pairing fluctuations. The dip structure eventually vanishes at a certain temperature, which we define as the pseudogap temperature T^* [40].

Figure 7 shows the resulting pseudogap temperature T^* in the BCS-BEC crossover. Starting from the weak-coupling BCS regime, T^* monotonically increases. However, T^* is still lower than T_c calculated in the mean-field BCS theory ("BCS" in Fig. 7). Although the mean-field T_c is sometimes considered as a characteristic temperature where preformed pairs are formed, our result shows that the pseudogap actually starts to develop in DOS from lower temperature.

We note that, although the fact that the pseudogap disappears at T^* is common to the entire BCS-BEC crossover region, the detailed way of disappearance is somehow different in between the BCS regime and crossover-BEC regime. In Fig. 5(a), the pseudogap around $\omega=0$ is simply filled up at high temperatures. The shape of DOS then becomes close to DOS of a free Fermi gas

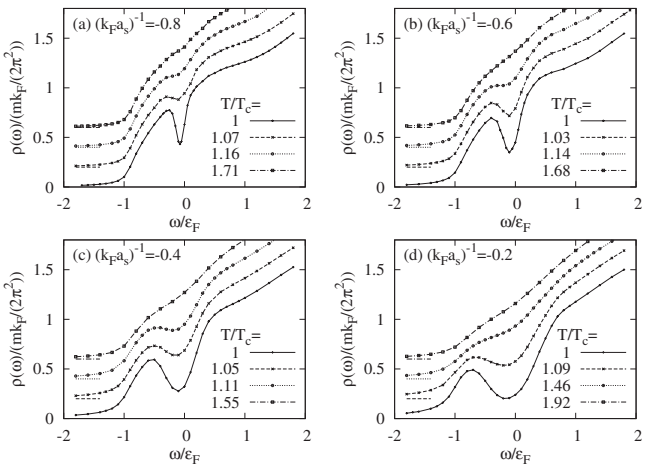

FIG. 5. Temperature dependence of the density of states $\rho(\omega)$ in the BCS side. T_c in each panel equals (a) $0.112\varepsilon_F$, (b) $0.146\varepsilon_F$, (c) $0.183\varepsilon_F$, and (d) $0.217\varepsilon_F$. In this figure and Fig. 6, we have offset the results for $T>T_c$. The short horizontal line near each result is at $\rho(\omega)=0$.

$$\rho(\omega)=\frac{m^{3/2}}{\sqrt{2}\pi^2}\sqrt{\omega+\mu}\quad(\omega\geq-\mu). \tag{19}$$

Namely, as far as we consider DOS, the system may be regarded as a (weakly interacting) normal Fermi gas above T^*. On the other hand, in the BEC side shown in Fig. 6, in addition to the enhancement of DOS around $\omega=0$, the lower peak is suppressed at high temperatures. In the unitarity limit [Fig. 6(a)], when the pseudogap is completely filled up, DOS still has a different shape from DOS of a free Fermi gas. In the BEC regime where $\mu<0$, Figs. 6(c) and 6(d) show that DOS above T^* has a finite intensity in the negative-energy region, in contrast to Eq. (17). These results indicate that pairing fluctuations still affect single-particle excitations above T^* in the BEC side, although the depression of DOS around $\omega=0$ is absent. Indeed, in Sec. IV, we will show an evidence of such fluctuation effects in the spectral weight in this regime.

IV. PSEUDOGAP IN SPECTRAL WEIGHT

It has been pointed out [21–24] that pairing fluctuations cause a BCS-type double-peak structure in the single-particle spectral weight $A(\boldsymbol{p},\omega)$. In this section, we examine how this strong-coupling effect is related to the pseudogap in DOS discussed in Sec. III.

Figure 8 shows the intensity of spectral weight $A(\boldsymbol{p},\omega)$ at T_c in the energy-momentum plane. In the BCS side [Fig. 8(a)], in addition to the particle branch at $\omega\simeq\xi_{\boldsymbol{p}}$, we can see

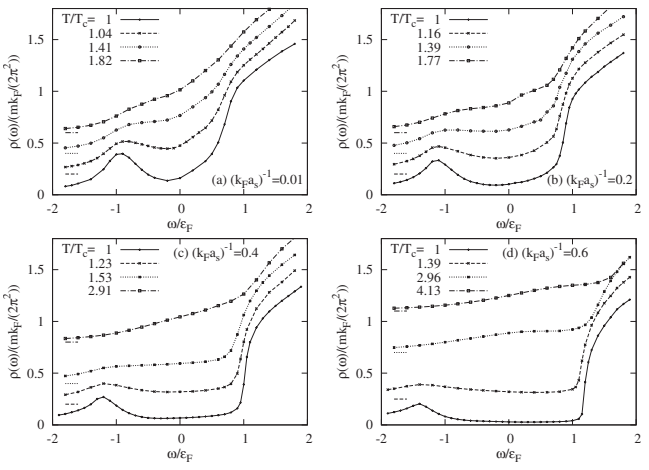

FIG. 6. Temperature dependence of DOS in the BEC side. T_c in each panel equals (a) $0.244\varepsilon_F$, (b) $0.259\varepsilon_F$, (c) $0.262\varepsilon_F$, and (d) $0.255\varepsilon_F$.

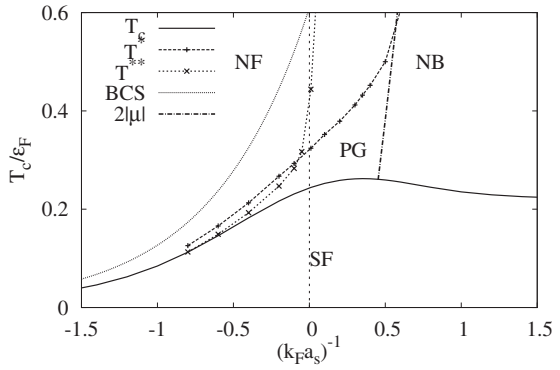

FIG. 7. Pseudogap temperature T^* determined from DOS in the BCS-BEC crossover. We also plot another pseudogap temperature T^{**} where the double-peak structure in the spectral weight vanishes. "BCS" is $T_c=(8\gamma/\pi e^2)\varepsilon_F e^{\pi/2k_F a_s}$ in the mean-field BCS theory (where $\gamma=1.78$) [39]. T^* or T^{**} gives the boundary between the pseudogap regime (PG) and normal Fermi gas regime (NF). $2|\mu|$ ($\simeq E_{\rm bind}$) in the BEC regime gives the characteristic temperature below which thermal dissociation of bound molecules is suppressed. Namely, $T\simeq 2|\mu|$ physically describes the boundary between PG and normal Bose gas regime (NB).

a weak peak line of a hole branch at $\omega\simeq-\xi_p$. The intensity of the particle branch is suppressed around $\omega=0$, where it intersects with the hole branch and the level repulsion between them occurs. The resulting structure is similar to the BCS spectral weight [21–24,41] given by [38]

$$A_{\rm BCS}(\boldsymbol{p},\omega)=u_p^2\delta(\omega-E_p)+v_p^2\delta(\omega+E_p), \qquad (20)$$

where $u_p^2=(1+\xi_p/E_p)/2$, $v_p^2=(1-\xi_p/E_p)/2$, and $E_p=\sqrt{\xi_p^2+\Delta^2}$ is the Bogoliubov quasiparticle excitation spectrum. For a given momentum p, $A_{\rm BCS}(\boldsymbol{p},\omega)$ has two peaks at $\omega=\pm E_p$. The negative-energy branch at $\omega=-E_p$ given by the second term in Eq. (20) is dominant in the low-momentum region $p\ll p_F$ (where $u_p\ll v_p$). On the other hand, the positive-energy branch ($\omega=+E_p$) becomes crucial when $p\gg k_F$ (where $u_p\gg v_p$). The existence of two branches can be understood from the Bogoliubov transformation $c_{p\uparrow}=u_p\gamma_{p\uparrow}+v_p\gamma^\dagger_{-p\downarrow}$ ($\gamma_{p\sigma}$ is an annihilation operator of a quasiparticle with momentum

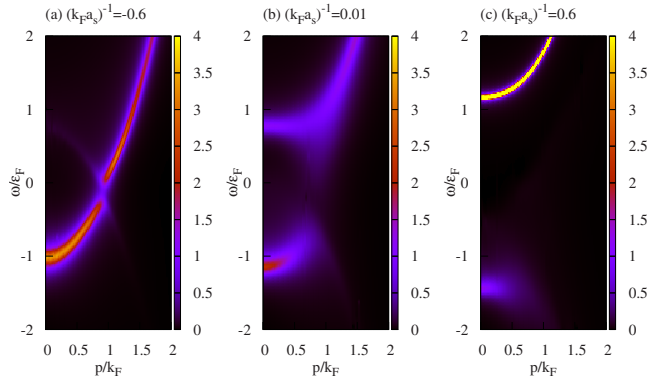

FIG. 8. (Color online) Calculated intensity of the spectral weight $A(\boldsymbol{p},\omega)$ at T_c in the energy-momentum plane. (a) BCS side $[(k_F a_s)^{-1}=-0.6]$. (b) Unitarity limit $[(k_F a_s)^{-1}=0.01]$. (c) BEC side $[(k_F a_s)^{-1}=0.6]$.

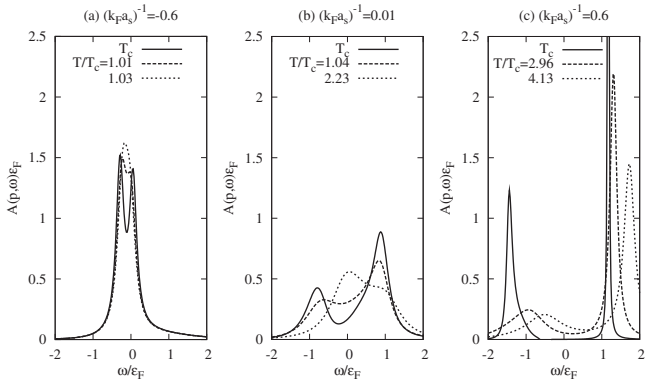

FIG. 9. Spectral weight $A(\boldsymbol{p},\omega)$ as a function of ω. In each panel, we take the momentum where the peak-to-peak energy becomes minimum: (a) $p/k_F=0.91$, (b) 0.83, and (c) 0.01.

$\boldsymbol{p}$ and spin σ), which indicates that the annihilation of an atom is accompanied by creation and annihilation of Bogoliubov excitations [42]. The minimum energy gap 2Δ between the two branches $\omega=\pm E_p$ is obtained at the Fermi level $p=k_F$. Since the simplified Green's function in Eq. (16) has the same form as Eq. (14), Eq. (16) gives rise to the spectral weight similar to the BCS type in Eq. (20), where the superfluid gap Δ is now replaced with the pseudogap $\Delta_{\rm pg}$, describing effects of pairing fluctuation. The minimum value $2\Delta_{\rm pg}$ of the pseudogap energy is obtained at $p\simeq k_F$ in this case. From this reason, the double-peak structure in Fig. 8(a) is found to come from the particle-hole coupling due to strong pairing fluctuations [24]. In addition, they also induce finite lifetime of quasiparticle excitations, leading to finite widths of the two peaks in $A(\boldsymbol{p},\omega)$ [24]. This feature is absent in the BCS spectral weight in Eq. (20), which has two δ-functional peaks at $\omega=\pm E_p$. As a result, $A(\boldsymbol{p},\omega)$ at the momentum where the minimum peak-to-peak energy is obtained has finite spectral weight between the two peaks, as shown in Fig. 9, giving a finite intensity of DOS inside the pseudogap. This *gapless* double-peak structure is referred to as the pseudogap in the spectral weight in the literature [21–24].

This pseudogap structure in the spectral weight becomes remarkable, as one approaches the unitarity limit. In this limit, strong pairing fluctuations also broaden the spectral peaks, as shown in Fig. 8(b). In the BEC regime [Fig. 8(c)], the peak width of the upper branch shrinks. This is because the BEC regime is well described by a gas of tightly bound molecules, so that the upper branch simply describes their dissociation. Since the molecular formation simply occurs within two-body physics in the BEC limit, the peak of the lower branch (which is an evidence of many-body physics) is low and broad in Fig. 8(c).

These different behaviors of upper and lower peaks in the BEC regime can be directly understood from the imaginary part of the self-energy correction. Using the fact that the particle-particle scattering matrix Γ reduces to the Bose Green's function in the BEC limit as [24]

$$\Gamma(\boldsymbol{q}, i\nu_n) = \frac{8\pi}{m^2 a_s} \frac{1}{i\nu_n - E_{\boldsymbol{q}}^B} \tag{21}$$

[where $E_{\boldsymbol{q}}^B = q^2/4m - \mu_B$ is the energy of a molecule measured from the molecular chemical potential $\mu_B \simeq 2\mu + 1/(ma_s^2) \simeq 0$], we can approximately evaluate the imaginary part of the analytical continued self-energy in Eq. (12) as

$$\begin{aligned} \mathrm{Im}\,\Sigma(\boldsymbol{p}, \omega + i\delta) &= -\frac{8\pi^2}{m^2 a_s} \sum_{\boldsymbol{q}} n_B(E_{\boldsymbol{q}}^B)\, \delta(\omega - (E_{\boldsymbol{q}}^B - \xi_{\boldsymbol{q}-\boldsymbol{p}})), \\ &= -\frac{4T}{a_s p} \ln \left[\frac{1 - \exp\left\{ -\beta \left(\frac{3p^2}{2m} + \Delta\omega + \frac{2p}{\sqrt{m}} \sqrt{\frac{p^2}{2m} + \Delta\omega} - \mu_B \right) \right\}}{1 - \exp\left\{ -\beta \left(\frac{3p^2}{2m} + \Delta\omega - \frac{2p}{\sqrt{m}} \sqrt{\frac{p^2}{2m} + \Delta\omega} - \mu_B \right) \right\}} \right] \theta\left(\frac{p^2}{2m} + \omega_{\mathrm{th}} - \omega \right), \end{aligned} \tag{22}$$

where $\Delta\omega = \omega_{\mathrm{th}} - \omega$ and $\omega_{\mathrm{th}} = \mu - \mu_B \simeq -1/2ma_s^2$. Since $\mathrm{Im}\,\Sigma(\boldsymbol{p}, \omega + i\delta)$ directly gives the peak width of the spectral weight, the first line in Eq. (22) indicates that, in the BEC regime, the peak widths are dominated by molecules excited thermally with finite center-of-mass momentum $\boldsymbol{q} \neq 0$. Since Eq. (22) vanishes when $\omega > p^2/2m + \omega_{\mathrm{th}} \simeq p^2/2m - 1/2ma_s^2$, the upper branch around $\omega = \xi_{\boldsymbol{p}} (> 0)$ appears as a sharp delta-function peak in the spectral weight in the BEC limit. This is consistent with the sharp upper peak in Fig. 9(c).

On the other hand, expanding Eq. (22) around the lower branch, $\omega = \xi_{\boldsymbol{p}}$, one obtains

$$\mathrm{Im}\,\Sigma(\boldsymbol{p}, \omega + i\delta) \simeq \frac{4T}{a_s p} \ln\left(\frac{m}{4Tp^2} \delta\omega^2 \right), \tag{23}$$

where $\delta\omega = \omega - (-\xi_{\boldsymbol{p}})$. Equation (23) shows that the imaginary part of the self-energy logarithmically diverges along the lower branch $\omega = -\xi_{\boldsymbol{p}}$. Thus, the lower peak is smeared out in the BEC limit.

As one increases the temperature, Fig. 9 shows that the double-peak structure gradually becomes obscure to eventually vanish at a certain temperature ($\equiv T^{**}$). Regarding T^{**} as another pseudogap temperature [43], one might expect that it is deeply related to T^* defined from DOS, because DOS is given by the momentum summation of the spectral weight. However, when we compare T^{**} with T^* in the BCS-BEC crossover, they are very different from each other, as shown in Fig. 7. While one sees $T^* > T^{**}$ in the BCS side [21], T^{**} becomes higher than T^* in the BEC side [$(k_F a_s)^{-1} \gtrsim -0.07$].

In the BCS side, when $T \gtrsim T^{**}$, since pairing fluctuations are still strong near the Fermi surface, the single peak in the spectral weight at $p \simeq \sqrt{2m\mu}$ is broad and the peak height is low, compared with the cases of higher and lower momenta, as shown in Fig. 10. This low peak height at $p \simeq \sqrt{2m\mu}$ directly affects the density of states around $\omega = 0$, leading to the dip or pseudogap structure in $\rho(\omega)$ in the region $T^{**} \leq T \leq T^*$. We briefly note that the result of $T^* > T^{**}$ in the BCS side agrees with the previous work [21].

On the other hand, although the double-peak structure still exists when $T > T^*$ in the BEC side, the intensity of the lower peak is very weak and broad (see Fig. 11) because the system is close to a gas of two-body bound molecules. Thus, the existence of lower peak is easily smeared out in the momen-

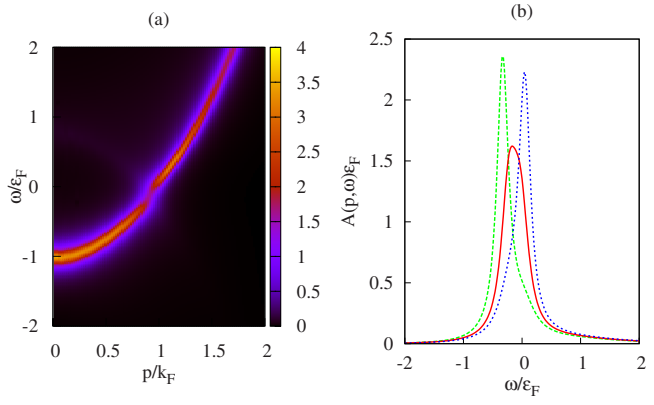

FIG. 10. (Color online) (a) Intensity of the spectral weight $A(\boldsymbol{p}, \omega)$ in the BCS side [$(k_F a_s)^{-1} = -0.6$]. We set $T/T_c = 1.03$, at which the dip structure can be clearly seen in DOS. (b) $A(\boldsymbol{p}, \omega)$ as a function of ω. The momentum p is taken to be $p/k_F = 0.91$ (solid line), 0.83 (dashed line), and 0.97 (dotted line).

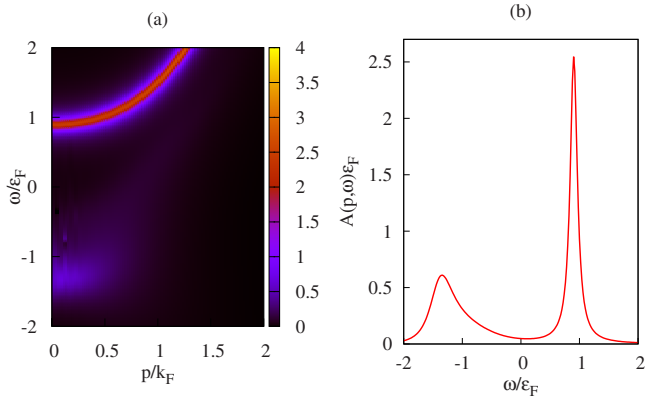

FIG. 11. (Color online) (a) Intensity of spectral weight $A(\boldsymbol{p}, \omega)$ in the BEC side [$(k_F a_s)^{-1} = +0.4$]. We take $T/T_c = 1.53$, at which the pseudogap structure is absent in DOS. (b) $A(\boldsymbol{p}, \omega)$ as a function of ω at $p = 0.01 k_F$.

tum summation in calculating DOS, $\rho(\omega)=\Sigma_{\boldsymbol{p}}A(\boldsymbol{p},\omega)$.

To see the physical backgrounds of T^* and T^{**}, it is convenient to recall that, when pairs are formed above T_c, the lifetime of Fermi excitations becomes short due to strong tendency to form pairs, leading to a broad quasiparticle peak in the spectral weight $A(\boldsymbol{p},\omega)$. In addition, preformed pairs also induce the particle-hole coupling, which gives the double-peak structure in $A(\boldsymbol{p},\omega)$. Between the two effects associated with pair formation, while T^{**} is directly related to the latter by definition, the former is crucial for T^*: in the BCS regime, since the peak-to-peak energy in $A(\boldsymbol{p},\omega)$ is small, the double-peak pseudogap structure is easily smeared out by the lifetime effect, namely, the broadening of two peaks. On the other hand, DOS around $\omega=0$ is suppressed, when the height of quasiparticle peak at $\omega\simeq 0$ is lowered by the broadening effect. As a result, one obtains $T^*>T^{**}$ in the BCS regime, and one regard T^* as the characteristic temperature where preformed pairs appear. The double-peak structure can be clearly seen in $A(\boldsymbol{p},\omega)$ in the crossover-BEC regime, because the peak-to-peak energy becomes larger than the peak widths. However, as discussed previously, the lower peak becomes very broad and the weight becomes small in the BEC regime, reflecting that the system is close to a gas of two-body bound molecules. Thus, one cannot see the dip structure in DOS even when the particle-hole coupling induce the double-peak structure in $A(\boldsymbol{p},\omega)$ below T^{**}. As one further decrease the temperature, the lower peak in $A(\boldsymbol{p},\omega)$ shrinks and the peak height increases, because the system approaches the superfluid phase. This clearly enhances the intensity of DOS in the negative-energy region, leading to the dip structure below $T^*(<T^{**})$. Thus, T^{**} corresponds to the characteristic temperature of pair formation in the crossover-BEC regime.

The different behaviors of two pseudogap temperatures T^* and T^{**} imply that the pseudogap region may depend on what we measure. When we consider a quantity where DOS is crucial, T^* would give the boundary between the pseudogap region and normal Fermi gas regime. On the other hand, when we consider a quantity dominated by the spectral weight, T^{**} would be observed as the boundary between the two regions. While the specific heat is an example of the former quantity, the recent photoemission-type experiment [33] is considered to be a latter example.

We note that, when the temperature is lower than the binding energy $E_{\rm bind}\simeq 2|\mu|$ of a two-body bound molecule in the BEC regime, the thermal dissociation of molecules is suppressed. In this sense, one may regard this regime as a normal Bose gas, rather than a (strongly correlated) Fermi gas. Including this, we obtain the phase diagram in Fig. 7. In this figure, the pseudogap regime is the region surrounded by T^* or T^{**}, T_c, and $2|\mu|$. We briefly note that, except for T_c, other temperatures T^*, T^{**}, and $T=2|\mu|$ are all crossover temperatures without being accompanied by any phase transition.

V. SUMMARY

To summarize, we have investigated the pseudogap behaviors of an ultracold Fermi gas in the BCS-BEC crossover above T_c. We have calculated the single-particle density of states (DOS), as well as the single-particle spectral weight, including pair fluctuations within the framework of T-matrix approximation. We showed how the pseudogap structure appears or disappears in DOS above T_c in the BCS-BEC crossover region. Starting from the weak-coupling BCS regime, while the pseudogap in DOS becomes remarkable near the unitarity limit, it continuously changes into a fully gapped DOS in the BEC regime.

We determined the pseudogap temperature T^* as the temperature when the dip structure in DOS disappears. We also introduced another pseudogap temperature T^{**} at which the double-peak structure in the spectral weight vanishes. We showed that, although both the dip structures in DOS and the double-peak structure in the spectral weight originate from pairing fluctuations, their values are very different from each other in the BCS-BEC crossover. While one finds $T^*>T^{**}$ in the BCS side $[(k_Fa_s)^{-1}\lesssim 0]$, T^{**} becomes much higher than T^* in the BEC side $[(k_Fa_s)^{-1}\gtrsim 0]$. This means that the pseudogap region may depend on the physical quantities which we measure. In particular, since the recent photoemission-type experiment [33] is related to the spectral weight, one expects that T^{**} would work as the pseudogap temperature in this experiment. Including T^* and T^{**}, we determined the pseudogap region in the BCS-BEC phase diagram with respect to temperature and the strength of pairing interaction. Since the pseudogap effects are crucial in understanding strong-coupling Fermi superfluids, our results would be useful in the search for the pseudogap region in the BCS-BEC crossover regime of ultracold Fermi gases.

ACKNOWLEDGMENTS

We would like to thank A. Griffin for valuable discussions and comments. This work was supported by a Grant-in-Aid for Scientific research from MEXT in Japan (Contracts No. 18043005 and No. 20500044).

[1] D. M. Eagles, Phys. Rev. **186**, 456 (1969).
[2] A. J. Leggett, *Modern Trends in the Theory of Condensed Matter* (Springer, Berlin, 1980).
[3] P. Nozières and S. Schmitt-Rink, J. Low Temp. Phys. **59**, 195 (1985).
[4] C. A. R. Sá de Melo, M. Randeria, and J. R. Engelbrecht, Phys. Rev. Lett. **71**, 3202 (1993).
[5] C. A. Regal, M. Greiner, and D. S. Jin, Phys. Rev. Lett. **92**, 040403 (2004).
[6] M. W. Zwierlein, C. A. Stan, C. H. Schunck, S. M. F. Raupach, A. J. Kerman, and W. Ketterle, Phys. Rev. Lett. **92**, 120403 (2004).

[7] J. Kinast, S. L. Hemmer, M. E. Gehm, A. Turlapov, and J. E. Thomas, Phys. Rev. Lett. **92**, 150402 (2004).
[8] M. Bartenstein, A. Altmeyer, S. Riedl, S. Jochim, C. Chin, J. H. Denschlag, and R. Grimm, Phys. Rev. Lett. **92**, 203201 (2004).
[9] W. Ketterle and M. W. Zwierlein, in *Proceedings of the International School of Physics "Enrico Fermi"*, edited by M. Inguscio, W. Ketterle, and C. Salomon (IOS Press, Amsterdam, 2008), Course CLXIV.
[10] E. Timmermans, K. Furuya, P. W. Milonni, and A. K. Kerman, Phys. Lett. A **285**, 228 (2001).
[11] M. Holland, S. J. J. M. F. Kokkelmans, M. L. Chiofalo, and R. Walser, Phys. Rev. Lett. **87**, 120406 (2001).
[12] Y. Ohashi and A. Griffin, Phys. Rev. Lett. **89**, 130402 (2002).
[13] S. Giorgini, L. Pitaevskii, and S. Stringari, Rev. Mod. Phys. **80**, 1215 (2008).
[14] I. Bloch, J. Dalibard, and W. Zwerger, Rev. Mod. Phys. **80**, 885 (2008).
[15] P. Lee, N. Nagaosa, and X. Wen, Rev. Mod. Phys. **78**, 17 (2006).
[16] O. Fischer, M. Kugler, I. Maggio-Aprile, C. Berthod, and C. Renner, Rev. Mod. Phys. **79**, 353 (2007).
[17] H. Yasuoka, T. Imai, and T. Shimizu, *Strong Correlation and Superconductivity* (Springer-Verlag, Berlin, 1989).
[18] A. Damascelli, Z. Hussain, and Z. Shen, Rev. Mod. Phys. **75**, 473 (2003).
[19] M. Randeria, N. Trivedi, A. Moreo, and R. T. Scalettar, Phys. Rev. Lett. **69**, 2001 (1992).
[20] J. M. Singer, M. H. Pedersen, T. Schneider, H. Beck, and H.-G. Matuttis, Phys. Rev. B **54**, 1286 (1996).
[21] B. Jankó, J. Maly, and K. Levin, Phys. Rev. B **56**, R11407 (1997).
[22] D. Rohe and W. Metzner, Phys. Rev. B **63**, 224509 (2001).
[23] Y. Yanase and K. Yamada, J. Phys. Soc. Jpn. **70**, 1659 (2001).
[24] A. Perali, P. Pieri, G. C. Strinati, and C. Castellani, Phys. Rev. B **66**, 024510 (2002).
[25] D. Pines, Z. Phys. B: Condens. Matter **103**, 129 (1997), and references therein.
[26] A. Kampf and J. R. Schrieffer, Phys. Rev. B **41**, 6399 (1990).
[27] S. Chakravarty, R. B. Laughlin, D. K. Morr, and C. Nayak, Phys. Rev. B **63**, 094503 (2001).
[28] P. Pieri, L. Pisani, and G. C. Strinati, Phys. Rev. Lett. **92**, 110401 (2004); Phys. Rev. B **70**, 094508 (2004).
[29] G. M. Bruun and G. Baym, Phys. Rev. A **74**, 033623 (2006).
[30] P. Massignan, G. M. Bruun, and H. T. C. Stoof, Phys. Rev. A **78**, 031602(R) (2008).
[31] Q. Chen and K. Levin, Phys. Rev. Lett. **102**, 190402 (2009).
[32] R. Haussmann, M. Punk, and W. Zwerger, e-print arXiv:0904.1333.
[33] J. T. Stewart, J. P. Gaebler, and D. S. Jin, Nature (London) **454**, 744 (2008).
[34] M. Randeria, in *Bose-Einstein Condensation*, edited by A. Griffin, D. W. Snoke, and S. Stringari (Cambridge University Press, New York, 1995), p. 355.
[35] T. L. Ho, Phys. Rev. Lett. **92**, 090402 (2004).
[36] D. J. Thouless, Ann. Phys. (N.Y.) **10**, 553 (1960).
[37] S. Tsuchiya, R. Watanabe, and Y. Ohashi, Autumn Meeting of Physical Society of Japan, 2008 (unpublished).
[38] G. D. Mahan, *Many-Particle Physics* (Kluwer Academic, Plenum Publishers, New York, 2000).
[39] C. J. Pethick and H. Smith, *Bose-Einstein Condensation in Dilute Gases* (Cambridge University Press, Cambridge, England, 2002).
[40] In this paper, we determine T^* as the temperature when the region of $d\rho(\omega)/d\omega<0$ disappears.
[41] When we plot $A_{\mathrm{BCS}}(\boldsymbol{p},\omega)$ in the energy-momentum plane, the BCS gap symmetrically appears as $\omega=\pm\Delta$ at $p=k_{\mathrm{F}}$. In Fig. 8(a), although the region where the peak line is suppressed is not symmetric with respect to $\omega=0$, this is simply due to the noninteracting Green's function $G^0_{\boldsymbol{p}(i\omega_n)}$ used to calculate the self-energy. When the shift of the chemical potential by the self-energy correction is correctly included in $G^0_{\boldsymbol{p}(i\omega_n)}$, it has been shown that the pseudogapped region in $A(\boldsymbol{p},\omega)$ appears symmetrically with respect to $\omega=0$. For more details, see Ref. [24].
[42] A. Griffin (private communication).
[43] In this paper, we determine T^{**} as the temperature when the double-peak structure of $A(\boldsymbol{p},\omega)$ at $p=\sqrt{2m\mu}$ vanishes, when $\mu>0$. In the BEC regime where $\mu\leq 0$, we use the spectral weight at $p=0$ for this purpose.